

## Synergistically Enhanced Electrochemical (ORR) Activity of Graphene Oxide, Using Boronic Acid as an Interlayer Spacer

Ehsan Pourazadi,<sup>a</sup> Enamul Haque,<sup>a</sup> Weimin Zhang,<sup>a</sup> Andrew T. Harris<sup>a</sup> and Andrew I. Minett,<sup>a\*</sup>

## Section.1

### Materials:

All chemicals were purchased from Sigma-Aldrich (unless otherwise stated) and used without additional purifications and refinements. Please note that, the identification of suppliers implies neither recommendation by the National Institute of Standard and Technology, nor that these chemicals or instruments are the superlatives.

### Graphene Oxide (GO) Synthesis:

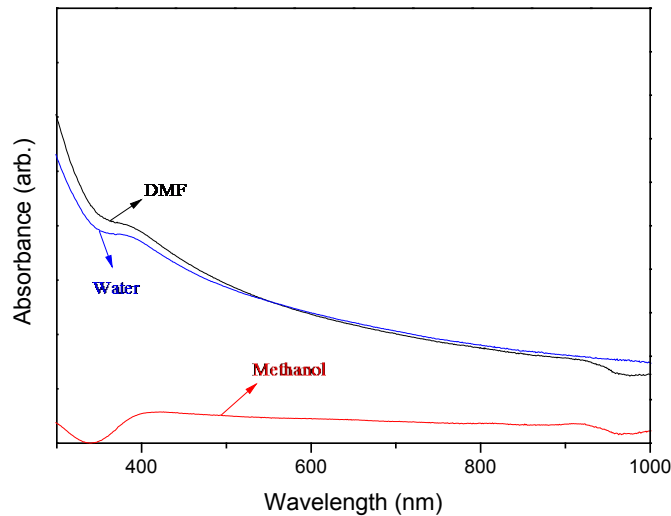
Graphene oxide was synthesized in four consecutive steps as follow;

1. Firstly, naturally expandable graphite flakes (Asbury Carbons, Grade: 3772, Carbon content: 99%) were thermally expanded at  $1050 \pm 2$  °C in a tube furnace for 15 seconds to obtain expandable graphite.
2.  $1 \pm 0.001$  g of expandable graphite and  $200 \pm 10$  mL  $H_2SO_4$  (98%) was stirred in a three-neck flask for 24 h. Then  $5 \pm 0.001$  g of  $KMnO_4$  (99.5%) was added to the mixture very cautiously and stirred at room temperature for the next 24 h.
3. The mixture was then cooled into an ice bath and  $200 \pm 10$  mL deionized water plus  $50 \pm 1$  mL  $H_2O_2$  (30%) were added dropwise via titration pipette, resulted in a color change to light brown (stirring for 30 min).
4. The final nanoparticle dispersion was washed and centrifuged at 6000 rpm three times with HCl (36%) solution (9:1 vol water: HCl), until a solution pH around 6 was achieved. The precipitations were collected and rinsed thoroughly with Milli-Q to be dried at  $80 \pm 2$  °C in vacuum oven for 24h.

### Graphene-Organic Framework (GOF) Synthesis:

#### Identification of proper solvent:

Our concern regarding maximization of GOF synthesis efficiency was followed by identification of the best solvent for GO exfoliation and hence, stitching of separated GO sheets to form GOF structure. Basically, different available solvents in our lab (i.e. methanol, ethanol, water, *N,N*-dimethylformamide (DMF) and etc.) were used for GO dispersion and the results evaluated for UV absorbance range of 300-1000 nm, using a Varian Cary 50UV UV-Visible spectrophotometer. DMF and also water indicated higher absorption capacity within whole range of transmissions (Fig.S1) compared to methanol which was used previously for GOF synthesis.<sup>1</sup> Basically, we considered DMF as the solvent medium since it provided highly stable and homogenous suspension of GO.



**FigS1.** UV-vis absorption results of as-prepared GO dispersion in methanol, water and DMF with  $0.50 \pm 0.01$  mg GO in 1 mL solvent (using bath sonicator for 1h). The spectra were gathered after 2h of stabilization.

#### GOF synthesis procedure and d-spacing characterization:

In a typical synthesis step, about  $5 \pm 0.01$  mg of GO was added to  $10 \pm 1$  mL of DMF and sonicated in an ice bath for nearly 1 h. Subsequently, different mass ratios of benzene 1,4-diboronic acid to GO (0.25:1, 0.50:1, 0.75:1 and 1:1) were mixed to suspensions. Mixtures with different linker ratios were transferred into 50 mL teflon reactors and sealed in stainless steel holders to be placed in oven at temperature of  $80 \pm 2$  °C for 5h. After completion of reaction, the samples were taken from oven and allowed to cool down at room temperature before to be filtered and washed with enough DMF to remove the residual unreacted boronic acid from the final materials. The stuffs were dried at  $60 \pm 2$  °C overnight and the final paper-like materials were cut for XRD characterization.

Successful linker anchoring into GO structure for additional d-spacing was evaluated by Bragg's law and Scherrer formula, using X-ray diffraction (Shimadzu S6000, CuK $\alpha$  radiation with Cu-K $\alpha$  radiation) peaks. Note that, the singularity of XRD peaks within the whole domain of  $2\theta=4-60^\circ$  revealed that our samples were solitarily contain single phase GOF. In order to calculate the interlayer distances, a Lorentzian equation was fit to each peak and Bragg's angle as well as the FWHM ( $w$ ) were extracted from the fitted function for applying in;

$$\text{Bragg's law: } d_{\text{spacing}} = \frac{\lambda}{2 \sin \theta} \quad (1)$$

$$\text{Scherrer formula: } t = \frac{K\lambda}{\beta \cos \theta} \quad (2)$$

where K is the shape factor ( $\approx 0.94$ )<sup>2</sup>,  $\lambda$  is X-ray wavelength (0.1542 nm),  $\beta$  is the line broadening at half of the maximum intensity (FWHM/2) in radians,  $\theta$  is the Bragg angle ( $x_c/2$ ) also in radians and  $t$  is the mean size of the crystalline domains, which may be smaller or equal to the grain size.<sup>1</sup> The interlayer distance for GOF(1:1) was calculated to be 1.01 nm which resulted in a GOF crystal size with approximately 15 individual graphene layers (dividing the thickness,  $t$ , over  $d_{\text{spacing}}$ ). Fig.S2 shows simultaneously a typical Lorentzian curve with its coefficients and prove the superiority of DMF in maximization of  $d_{\text{spacing}}$  for GOF synthesis (the peak shifts to lower angle in case of DMF).

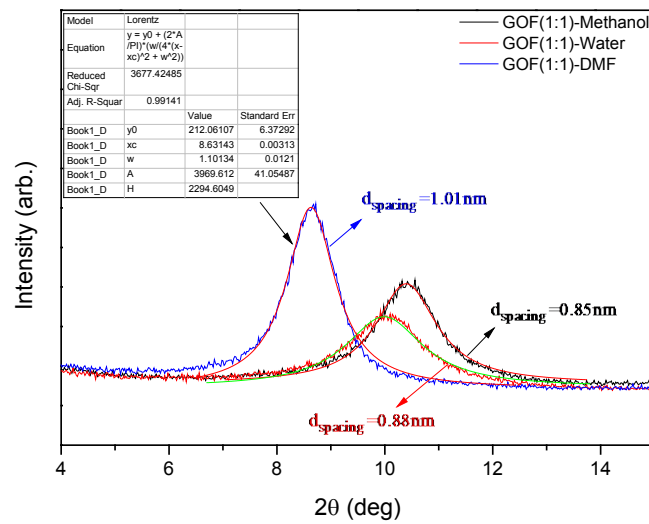


**Fig.S2** XRD patterns of synthesized GOFs(1:1) in different solvents and the fitted Lorentzian for employing Bragg's law and Scherrer formula.

Control sample (GO in DMF) was also prepared for comparison. The elemental composition was 71.40% C, 27.11% O, 1% N and 0.38% S based on the XPS result. The nitrogen peak was deconvoluted into two peaks, one at 401 eV and the other one at 402 eV corresponding to amino group, probably from entrapped DMF in sample.

Additional SEM (FESEM, Zeiss ultra Plus, 5 kV) images were taken from GO and synthesized GOF materials. The pictures clearly illustrate the compactness of layers in GO while GOF structure is more flaky with separate expanded sheets (Fig.S3a,b).

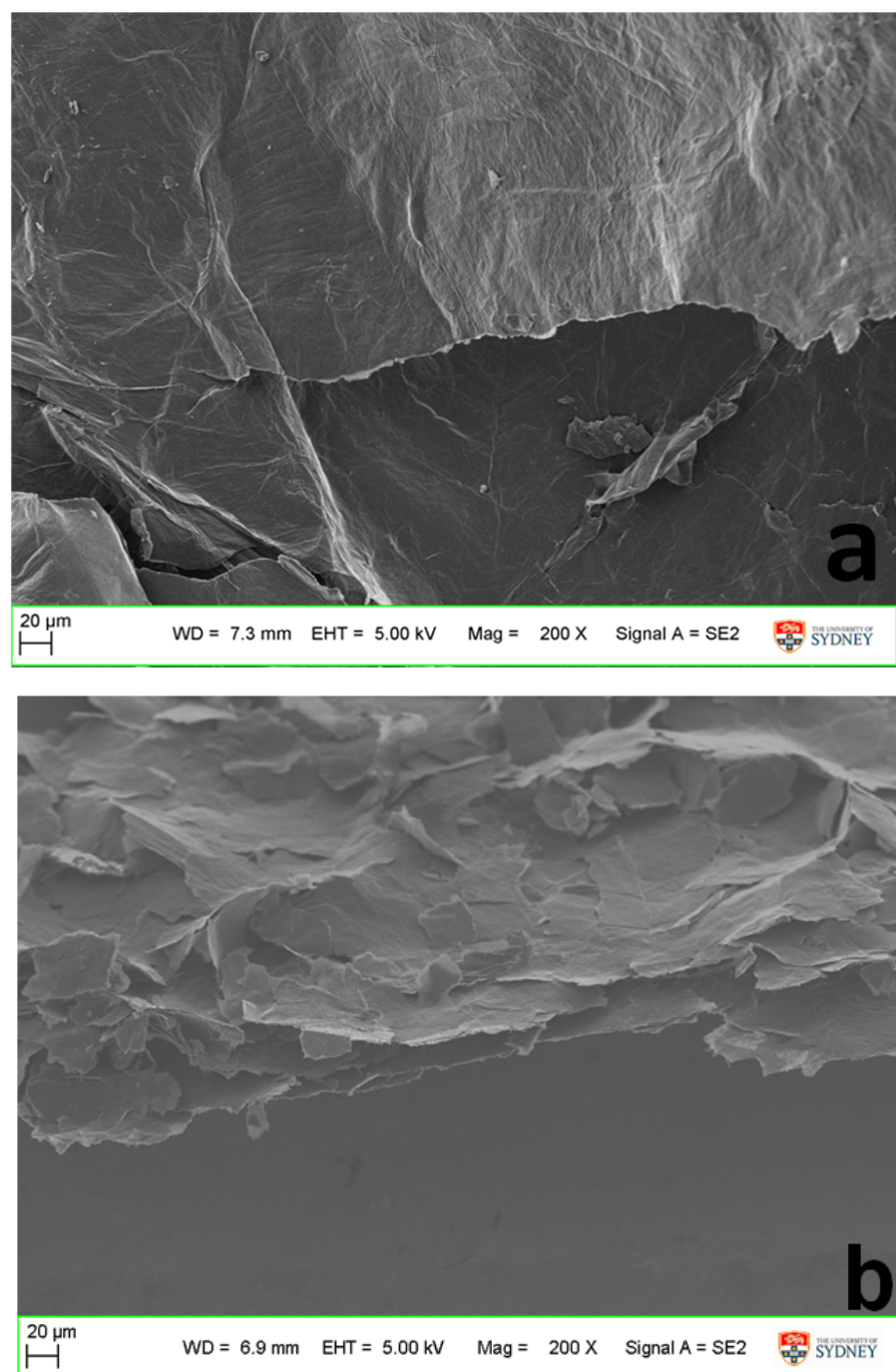


**Fig.S3** (a) magnified images for (a) GO and (b) typical GOF(1:1)

## Section.2

This part gives more illustrations of linker intercalation into GO structure during GOF synthesis.

### Thermogravimetric Analysis (TGA):

Thermal stability was studied using a thermogravimetric analyzer (TA Instruments, Q500) with ramping rate of  $2.5\text{ }^{\circ}\text{C min}^{-1}$  under  $\text{N}_2$  stream of  $60\text{ mL min}^{-1}$ . The results for thermal analysis of boronic acid, GOF(1:0.75), GOF(1:0.50) and air-dried GO precursor are demonstrated in Fig.S4.

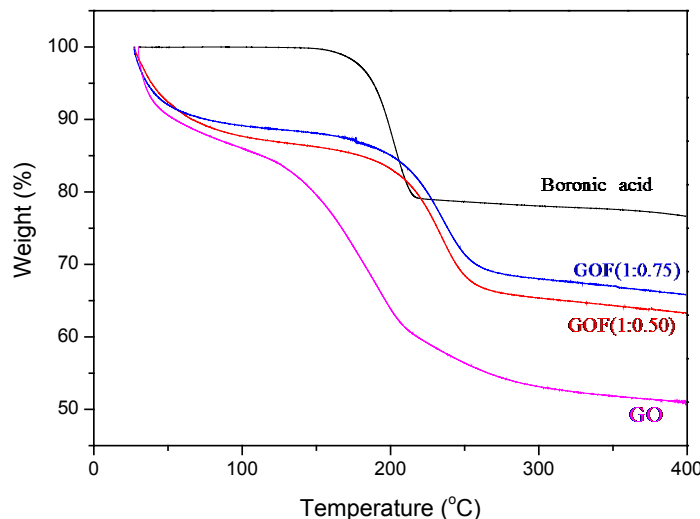


**Fig.S4** thermal stability analysis for benzene 1,4-diboronic acid, GO, GOF(1:0.75) and GOF(1:0.50) up to  $400\text{ }^{\circ}\text{C}$ .

All in all, the results indicated relative structural stability of GOFs compared to GO. All graphitic materials lose 10-15 wt% of their initial mass due to evaporation of entrapped water and probably solvent. The second 30 wt% mass reduction in GO is attributed to the pyrolysis of oxygen-containing functional groups. However, the decay for GOFs is not such restrict and it initiates after  $200\text{ }^{\circ}\text{C}$  (comparable with  $100\text{ }^{\circ}\text{C}$  for GO), which is demonstration of strong association of linkers to GO framework. As linker concentration increases, larger gap forms between GO sheets (see Fig.1a) which represents higher angles between linker and GO plane. From statically viewpoint, higher angles ( $\theta \rightarrow 90^{\circ}$ ) are followed by much more stability (compare the results for GOF(1:0.75) and GOF(1:0.50)).

### Raman Measurement:

Raman spectroscopy is a potent tool for investigating the structural changes of graphitic networks. Measurements were done by Raman spectrometer (InVia, Renishaw) using an Ar<sup>+</sup> ion 70 laser at  $\lambda=514.5$  nm. The spectra for both GO and GOF have a broad peak around  $1350\text{ cm}^{-1}$ , known as D band corresponding to the structural defects/disorders, and G band peak at  $1585\text{ cm}^{-1}$  for GO ( $1598\text{ cm}^{-1}$  for GOF(1:1)) which is attributed to in-plane vibration of sp<sup>2</sup> carbon=carbon bonds (Fig.S5). The relative intensity of  $\frac{I_G}{I_D}$  is approximately constant in case of GO and GOF which reveals no change in graphitic structure.<sup>3</sup>

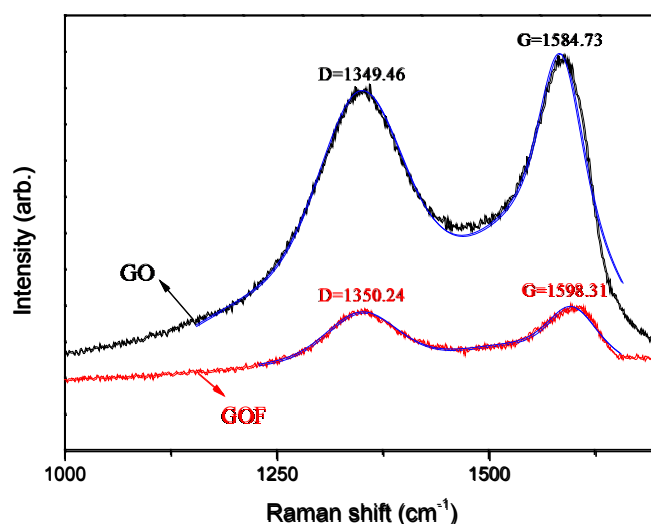


**Fig.S5** comparison of Raman D band and G band for GO and GOF (a combination of Lorentzian and Gaussian functions has been used for multiple fitting)

Chemical interaction between GO and electron donor/acceptor compounds is expected to change the density of sp<sup>2</sup>  $\pi$  electrons. Generally speaking, downshifts/up shifts have been observed for G band when GO comes to interact with the electron donors-acceptors dopants.<sup>4</sup> As it is clear, benzene 1,4-diboronic acid is a typical Lewis acid composed of deficient boron atoms which goes through esterification by reacting to GO hydroxyl groups as follows:<sup>1</sup>



Esterification of a typical boronic acid with the hydroxyl functional groups on GO surface

G: Graphene Oxide  
B: Boron

Basically, it is clear that boron acts as an electron acceptor from GO sheet which results in substantial blue shift (upshift) in the G band of GOF.

### Fourier Transform Infrared Spectroscopy (FTIR):

FTIR spectra (Fig.S6) were obtained via a Bruker IFS66V spectrometer. The relative intensity of C=C stretches to the C=O ones, remains constant for GO and GOF (1.04 vs. 1.05, respectively). This confirms that graphitic structure and correspondingly carboxylic stretches retain in GOFs. However, the broad peaks analogous to hydroxyl and epoxy groups (C-O) diminish due to combination of B with C-O functional groups. The peak at around  $670\text{ cm}^{-1}$  is assigned to the B-O covalent bonding based on the literature.<sup>1</sup> A wide peak is also observed around  $3500\text{ cm}^{-1}$ , which is assigned to O-H from water.<sup>1,3a,5</sup>

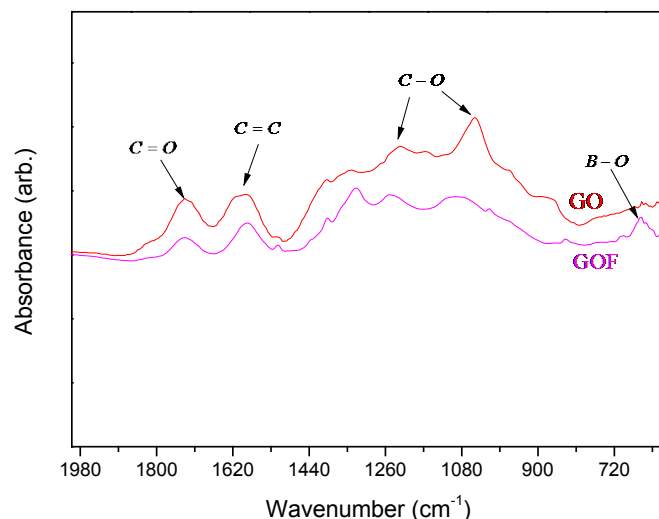


**Fig.S6** FT-IR absorbance for GO and GOF(1:1).

### X-Ray Photoelectron Spectroscopy (XPS):

X-ray photoelectron spectroscopy analysis was recorded with XPS, ESCALAB250Xi, Thermo scientific, UK (X-ray source: mono-chromated Al K alpha, Power: 164W (10.8 mA and 15.2kV) and binding energy reference: C1s = 285.0 eV for adventitious hydrocarbon) for examining the chemical states of different elements in GO and GOF(1:1) composites. The deconvoluted C1s peaks are presented here in Fig.S7a,b (see Fig.2 as well as Table.1 for more detail on XPS). Besides, based on the figures in Table.1 we got GOF-42, which is something between ideal GOF-32 and GOF-62. As n (number of graphene carbon per linker) in GOF-n increases, we will approach hypothetic single layer graphenes which have been separated by an absolute free space.<sup>1</sup>

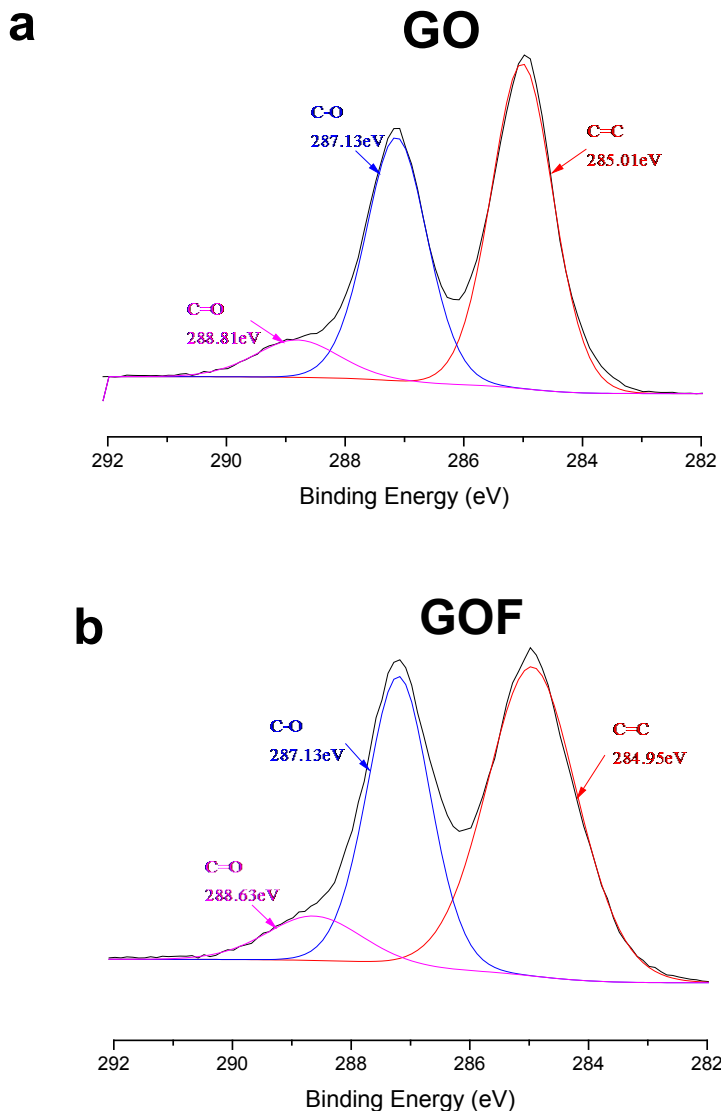


**Fig.S7** deconvoluted C1s peaks of GO and GOF(1:1)

It worth to mention that the downshift in XPS C=C peak position (from 285.01 to 284.95) confirms the  $\text{sp}^2$  C=C bond stiffening, observed by Raman spectra.<sup>4d</sup>

### Section.3

#### Electrochemical Characterizations:

All the electrochemical measurements were carried out at room temperature using a three-electrode system with GC electrode as working electrode, Pt wire as counter electrode and Ag/AgCl reference electrode filled with saturated 10%  $\text{KNO}_3$  solution (using Biologic SP300 digital potentiostat/galvanostat.). Cyclic voltammetry (CV) was typically performed at scan rate of  $10 \text{ mV s}^{-1}$ . The cyclic voltammogram experiments were conducted in 0.1 M KOH

solution which was purged with nitrogen or oxygen for 10 min prior to the electrochemical tests. In order to prepare the working electrode, GO and GOF were dispersed in mixture of 0.04 wt% Nafion, 5:1 wt% Isopropanol and water with 30 minutes sonication. 12  $\mu\text{L}$  of GO/GOF dispersion ( $1 \pm 0.01$  mg GO in  $1 \pm 0.01$  mL<sup>-1</sup> of Nafion solution) was dropped on glassy-carbon (GC) electrode with 5 mm diameter and 0.196 cm<sup>2</sup> geometrical area. The electrode was allowed to dry at room temperature for 20 min before tests. The CV and linear- scan-voltammetry (LSV) measurements were carried out using a Versastatwere 2-channel system (Princeton Applied Research). The same procedures were mimicked for electrode preparation and experiments in determining ORR activities.

Evaluation of kinetic parameters was completed with Koutecky-Levich plots, using the following relationship:

$$\frac{1}{i} = \frac{1}{i_k} + \frac{1}{B \cdot \omega^{1/2}} \quad (4)$$

where  $i$  is the measured current.  $i_k$  is the kinetic current and  $\omega$  is the electrode rotation rate in rpm. The theoretical value of the Levich slope (B) was evaluated from the following relationship:

$$B = 0.20nFC_{O_2}D_{O_2}^{2/3} \nu^{-1/6} \quad (5)$$

where n is the overall number of transferred electrons through ORR, F is the Faradiac constant (96485 C/mol),  $C_{O_2}$  is the oxygen concentration in 0.1M KOH ( $1.2 \times 10^{-6}$  mol cm<sup>-3</sup>),  $D_{O_2}$  is the oxygen diffusion coefficient in 0.1M KOH ( $1.73 \times 10^{-5}$  cm<sup>2</sup>s<sup>-1</sup>) and finally  $\nu$  is the kinematic viscosity of mentioned electrolyte ( $0.01$  cm<sup>2</sup>s<sup>-1</sup>).<sup>6</sup>

### Electrochemistry Measurements for Commercial Platinum Electrode

CV and RDE tests were also performed for commercial 20% platinum electrode to evaluate the results of GOF materials. The onset potential is about -125 mV while the number of transferred electron are calculated as high as 4.3 which shows facile reduction of oxygen under such circumstances.

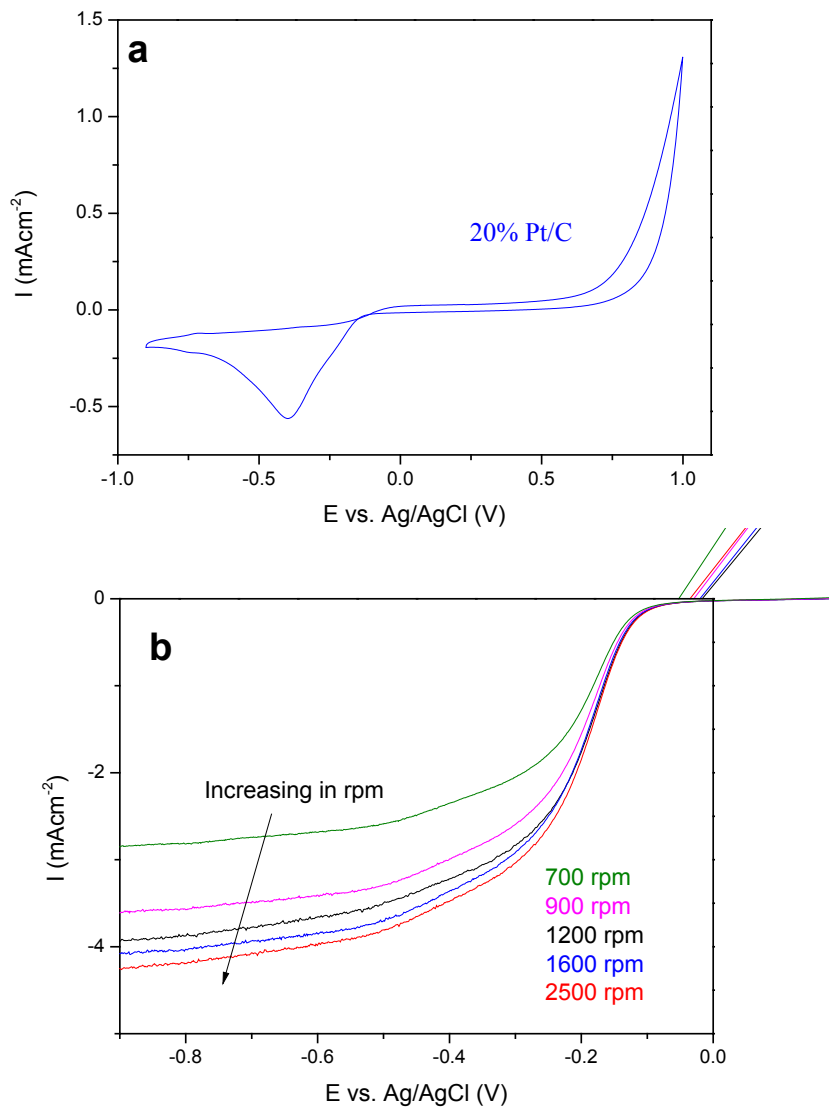


**Fig.S8** The results of CV and RDE measurements for commercial 20% Pt/C cathodic electrode.

**Supplementary Information References:**

1. J.W. Burress, S. Gadielli, J. Ford, J.M. Simmons, W. Zhou and T. Yildirim, *Angew. Chem. Int. Ed.* 2010, **49**, 8902.
2. (a) J.I. Langford and A.J.C. Wilson, *J Appl. Cryst.* 1978, **11**, 102; (b) P. Scherrer, *Göttinger Nachrichten Gesell.* 1918, **2**, 98; (c) B.D. Cullity, "Elements of X-Ray Diffraction", Addison-Wesley Publishing Company, Inc. 1956.
3. J. Han, L.L. Zhang, S. Lee, J. Oh, K.S. Lee, J.R. Potts, J. Ji, X. Zhao, R.S. Ruoff and S. Park, *ACS Nano.* 2013, **7**, 19; (b) W. Cai, R.D. Piner, F.J. Stadermann, S. Park, M.A. Shaibat, Y. Ishii, D. Yang, A. Velamakanni, S.J. An, M. Stoller, J. An, D. Chen and R.S. Ruoff, *Science*, 2008, **321**, 1815.
4. Q. Su, S. Pang, V. Aljani, C. Li, X. Feng and K. Mullen, *Adv. Mater.* 2009, **21**, 3191; (b) M.C. Hsiao, S.H. Liao, M.Y. Yen, P.I. Liu, N.W. Pu, C.A. Wang and C.M. Ma, *ACS Appl. Mater. Interfaces*, 2010, **2**, 3092; (c) A.M. Rao, P.C. Eklund, S. Bandow, A. Thess and R.E. Smalley, *Nature*, 1997, 388; (d) M.S. Dresselhaus and G. Dresselhaus, *Adv. Phys.* 1981, **30**, 139.
5. (a) M. Mermoux, Y. Chabre and A. Rousseau, *Carbon* 1991, **29**, 469; (b) C.H. Lucas, A.J. Lo'pez-Peinado, J. Lo'pez-Gonza'lez, M.L. Rojas-Cervantes and R.M. Martí'n-Aranda, *Carbon* 1995, **33**, 1585; (c) N.I. Kovtyukhova, P.J. Olliver, B.R. Martin, T.E. Mallouk, S.A. Chizhik, E.V. Buzaneva and A.D. Gorchinskiy, *Chem. Mater.* 1998, **11**, 771.
6. (a) M.K. Tham, R.D. Walker and K.E. Gubbins, *J. Phys. Chem.* 1970, **74**, 1747; (b) R.E. Davis, G.L. Horvath and C.W. Tobias, *Electrochim Acta*, 1967, **12**, 287; (c) Z. Lin, G.Waller, Y. Liu, M. Liu and C.P. Wong, *Adv. Energy Mater.* 2012, **2**, 884.